

Cramér–Rao lower bound of laser Doppler measurements at moving rough surfaces

This article has been downloaded from IOPscience. Please scroll down to see the full text article.

2011 Meas. Sci. Technol. 22 055301

(<http://iopscience.iop.org/0957-0233/22/5/055301>)

View [the table of contents for this issue](#), or go to the [journal homepage](#) for more

Download details:

IP Address: 141.30.5.252

The article was downloaded on 11/04/2011 at 08:36

Please note that [terms and conditions apply](#).

Cramér–Rao lower bound of laser Doppler measurements at moving rough surfaces

Thorsten Pfister, Andreas Fischer and Jürgen Czarske

Laboratory of Measurement and Testing Techniques, Department of Electrical Engineering and Information Technology, Technische Universität Dresden, Helmholtzstraße 18, 01062 Dresden, Germany

E-mail: thorsten.pfister@tu-dresden.de

Received 19 November 2010, in final form 13 February 2011

Published 8 April 2011

Online at stacks.iop.org/MST/22/055301

Abstract

Laser Doppler techniques are widely used for measuring both fluid flows and moving solid surfaces. The measurement uncertainty of laser Doppler sensors is fundamentally limited by the uncertainty of the Doppler frequency estimation. Generally, the minimum achievable uncertainty of any unbiased estimator is given by the Cramér–Rao lower bound (CRLB). While the CRLB is well known for laser Doppler burst signals of single tracer particles used in flow research, no analytical expression for the CRLB has been known up to now for scattered light signals of rough solid surfaces where speckle effects occur. Therefore, the aim of this paper is to close this gap and to provide a simple analytical expression for the CRLB for the Doppler frequency estimation from scattered light signals of moving rough solid surfaces for the first time. A comparison with experimental data demonstrates the validity of the derived analytical CRLB formula, which is also proven to be consistent with previous works. The progress for science is that this analytical CRLB formula enables both an easy estimation of the minimum achievable uncertainty of laser Doppler measurements at moving rough surfaces and a direct analysis of the influences of certain system and signal parameters on the measurement uncertainty. This reveals specific measuring features and capabilities of different laser Doppler techniques. In addition, the CRLB is a valuable tool to evaluate the efficiency of applied signal processing techniques.

Keywords: metrology, measurement and error theory, Cramér–Rao lower bound, laser Doppler techniques, moving rough surfaces, speckles, frequency estimation, velocity measurement, position and distance measurement

(Some figures in this article are in colour only in the electronic version)

1. Introduction

Laser Doppler velocimetry (LDV) was invented in 1964 by Yeh and Cummins [1]. Today it is a well-established technique not only for measuring velocities of small scattering particles in fluid flows [2, 3] but also for contactless and non-slip measurements of feed speed and length of moving solid goods, such as hot steel, sheet metals, wires, roofing fabric or foils [4, 5]. Mostly, LDV sensors are set up in differential configuration corresponding to a Mach–Zehnder interferometer, where an interference fringe system is

generated in the intersection volume of two crossing coherent laser beams constituting the measurement volume, see figure 1. The scattered light signal of an object (small particle or solid surface) passing through these interference fringes spaced at intervals of d exhibits an amplitude modulation with the Doppler frequency f_D , which is directly related to the transverse object velocity $v_x = f_D d$. The length of moving solids can be obtained by integrating the velocity v_x over time.

Furthermore, advanced and extended laser Doppler techniques were invented employing several superposed

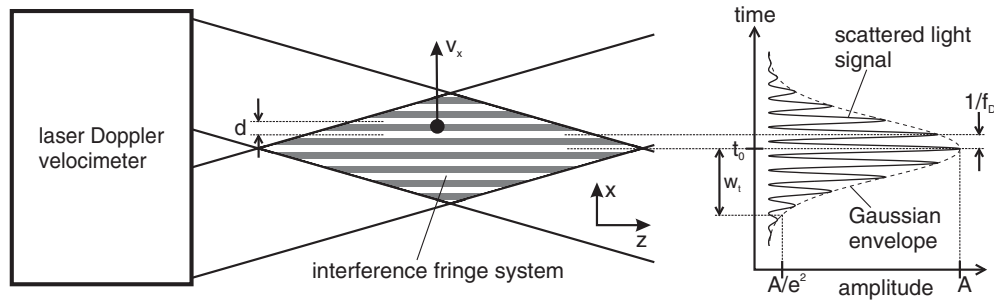


Figure 1. Working principle of a laser Doppler velocimeter for measuring the velocity v_x of a small scattering particle. On the right, the resulting scattered light signal is shown as an idealized model without noise.

but distinguishable interference fringe systems at the same location forming multiple measuring channels [2, 3]. Thus, not only multiple velocity components can be measured but also further measurands can be determined concurrently and independently, such as the axial position z of the object while passing through the interference fringes. For this purpose, recently, the laser Doppler distance sensor (LDDS) was invented which enables simultaneous measurement of both the axial position z and the transversal velocity v_x via two superposed fan-shaped interference fringe systems [6, 7]. This allows measuring the shape as well as eccentricity, deformations and vibrations of moving and rotating solids in particular [7–10]. Concerning fluid flows, velocity profiles e.g. within boundary layers can be determined instantaneously without traversing. For this reason, the LDDS is also referred to as laser Doppler velocity profile sensor [11–13].

In all laser Doppler techniques, the achievable measuring accuracy is fundamentally limited by the uncertainty of the Doppler frequency estimation σ_{f_D} . For conventional LDV, the relative velocity uncertainty can be expressed as [3]

$$\frac{\sigma_{v_x}}{v_x} = \sqrt{\left(\frac{\sigma_{f_D}}{f_D}\right)^2 + \left(\frac{\sigma_d}{d}\right)^2}. \quad (1)$$

Thus, even if there is no uncertainty in the fringe spacing d , i.e. $\sigma_d = 0$, which is impossible in practice because of the wave front curvature of Gaussian laser beams, the relative velocity uncertainty could not go below the relative uncertainty of the Doppler frequency estimation σ_{f_D}/f_D , which thus marks the lower limit. For the LDDS, the uncertainties for velocity and position measurements can be estimated by [6, 7]

$$\frac{\sigma_{v_x}}{v_x} \approx \sqrt{\frac{3}{2}} \cdot \frac{\sigma_{f_D}}{f_D} \quad \text{and} \quad \sigma_z \approx \frac{\sqrt{2}}{s} \cdot \frac{\sigma_{f_D}}{f_D}, \quad (2)$$

where s denotes the slope of the calibration curve. Here also, both uncertainties depend directly on the relative uncertainty of the Doppler frequency estimation σ_{f_D}/f_D . Consequently, it is crucial to know the minimum achievable uncertainty of the Doppler frequency estimation for judging the potential of a certain laser Doppler technique and for evaluating the efficiency of the signal processing techniques used. The solution to this problem is to determine the corresponding Cramér–Rao lower bound (CRLB), which defines the minimum achievable uncertainty of any unbiased estimator.

For noisy single-tone signals with constant amplitude, the CRLB for frequency estimation is well known [2, 14]. Also for estimating the Doppler frequency f_D of LDV burst signals of single scattering particles used in flow research, several analytical expressions for the CRLB have been derived under certain assumptions [15–18]. However, for scattered light signals of rough solid surfaces where disturbances due to speckle effects occur, no analytical expression for the minimum achievable uncertainty of the Doppler frequency estimation has been known up to now. Therefore, the aim of this paper is to close this gap by providing an analytical expression for the corresponding CRLB for the first time. Besides the benefit of allowing easy estimation of the minimum achievable uncertainty of LDV measurements at moving rough surfaces, this analytical expression directly reveals the influences of certain system and signal parameters on the attainable measurement uncertainty. Such information is important for analyzing and optimizing the measuring features of different laser Doppler sensors.

The paper is structured as follows. First, in section 2, an appropriate signal model for LDV scattered light signals of rough solid surfaces is derived including a discussion about relevant noise sources. In section 3, the general approach for calculating the CRLB is described, and it is shown how this calculation can be accomplished for the specific signal model introduced before. As a result, the CRLB for the Doppler frequency estimation from scattered light signals of rough solid surfaces is obtained. Afterward, in section 4, this analytical result is compared to experimental data using different signal processing techniques. Additionally, conclusions for the setup and for the application of laser Doppler sensors are discussed in section 5. Finally, the most important results are summarized in the last section.

2. Signal model

Generally, any detected scattered light signal $x[k]$, $k \in \{0, 1, \dots, N-1\}$, sampled with the sampling rate f_s can be written as

$$x[k] = m[k] + n[k], \quad (3)$$

where $m[k]$ is the undisturbed signal and $n[k]$ denotes the superposed noise. For calculating the CRLB, first of all, appropriate models for the undisturbed signal $m[k]$ as well as for the superposed noise are required. The model for the

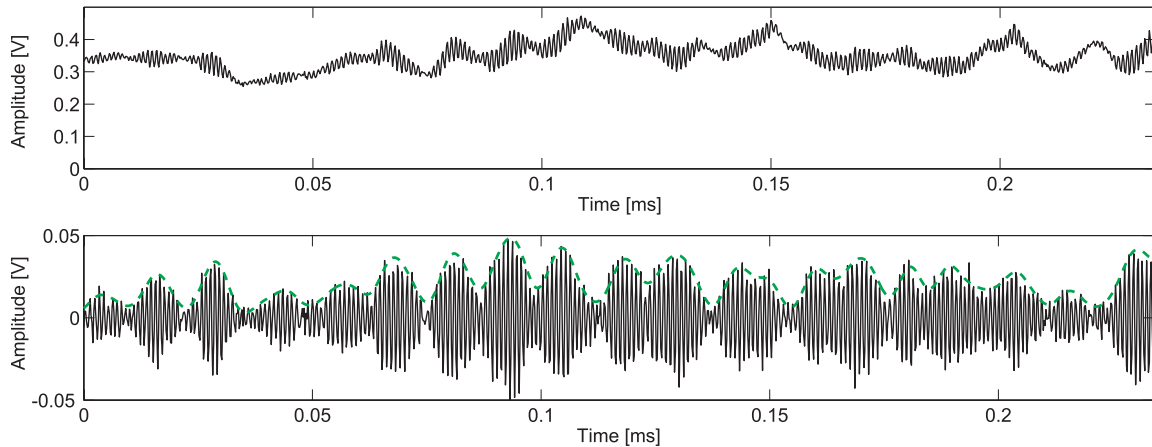


Figure 2. Top: segment of a measured LDV scattered light signal of a moving aluminum panel with a mean roughness index of $0.2 \mu\text{m}$. Bottom: corresponding high-pass-filtered signal without low-frequency part including envelope (dashed line).

undisturbed scattered light signal of a moving rough surface is based on the signal model for a single scattering particle, which is therefore described first.

2.1. Undisturbed signal of a single scattering particle

In the case of LDV, the undisturbed detector signal of a single scattering particle that crosses the measurement volume perpendicular to the interference fringes (cf figure 1) can be described by

$$\tilde{m}_s[k] = A e^{-\frac{2f_D^2(k/f_s - t_0)^2}{w^2}} [1 + \gamma \cos(2\pi f_D(k/f_s - t_0))], \quad k = 0, \dots, N_0 - 1, \quad (4)$$

with the amplitude A , the modulation depth $0 \leq \gamma \leq 1$ and the total number of samples N_0 . The parameter w designates half the interference fringe number $N_{\text{fringes}} = 2w$. Thus, it is related to the half temporal $1/e^2$ width of the Gaussian signal envelope $w_t = w/f_D$ and to the corresponding half lateral width of the interference fringe system $w_x = w \cdot d$. The particle arrival time t_0 denotes the time when the particle passes the center of the measurement volume (see figure 1). There is a fixed relationship between the Doppler modulation and the Gaussian envelope, which is physically given by the interference fringe system. Thus, the phase of the Doppler modulation is always the same in the middle of each burst signal where the Gaussian amplitude is maximal. The fringe spacing d is assumed to be constant within the measurement volume since the effect of fringe spacing variations will not be taken into account here. Also the object velocity v_x is assumed to be constant and accelerations are neglected accordingly.

As proven in appendix A.1, the low-frequency part of this signal corresponding to the first summand in equation (4) has no impact on the CRLB of the Doppler frequency estimation provided that the superposed noise can be assumed to be signal independent which is fulfilled here (see section 2.3). Thus, this low-frequency part can be neglected, and the signal model simplifies to

$$m_s[k] = \hat{A} e^{-\frac{2f_D^2(k/f_s - t_0)^2}{w^2}} \cos(2\pi f_D(k/f_s - t_0)), \quad k = 0, \dots, N_0 - 1, \quad (5)$$

with the peak value $\hat{A} = A\gamma$. Also in practice, the low-frequency part of the signal is normally not used for estimating the Doppler frequency f_D , but it is removed by electrical filters. In particular in heterodyne sensor setups with carrier frequency, this is done in the course of electrical mixing processes, where the signals are usually mixed down into the baseband for further evaluation. Hence, a carrier frequency is not explicitly considered here but can be easily included in the model by adding it to the Doppler frequency f_D inside the cosine term of equation (4).

The four unknown parameters of the signal $m_s[k]$ can be summarized in the vector

$$\vec{a}_s = (f_D, \hat{A}, w, t_0)^T. \quad (6)$$

2.2. Undisturbed scattered light signal of a moving rough solid surface

For LDV measurements on a moving rough solid surface, the signal shape is completely different as is visible in figure 2 [7, 19]. The reason is that the scattered light beams of many different coherently and simultaneously illuminated points on the rough surface are superposed in the detector plane with different amplitudes and phases resulting in constructive or destructive interference, respectively. Due to the random nature of rough surfaces, the resulting speckle pattern changes stochastically when the surface moves laterally (in the x -direction) through the illuminating interference fringes. In particular, for a lateral displacement of half a fringe spacing $d/2$, the speckle pattern changes almost completely [5]. The detector integrates the light intensity of this speckle pattern over the detector surface for each point in time. Due to this integration, the scattered light signal exhibits a relatively large offset which is varying only slightly and slowly over time compared to the Doppler modulation (see figure 2, top). This Doppler modulation is caused by the structured illumination with the interference fringe system. After removing the low-frequency part including the slowly varying offset using a high-pass filter, the remaining Doppler signal looks like a sequence of successive burst signals $m_{s,i}$, $i = 1, \dots, M$,

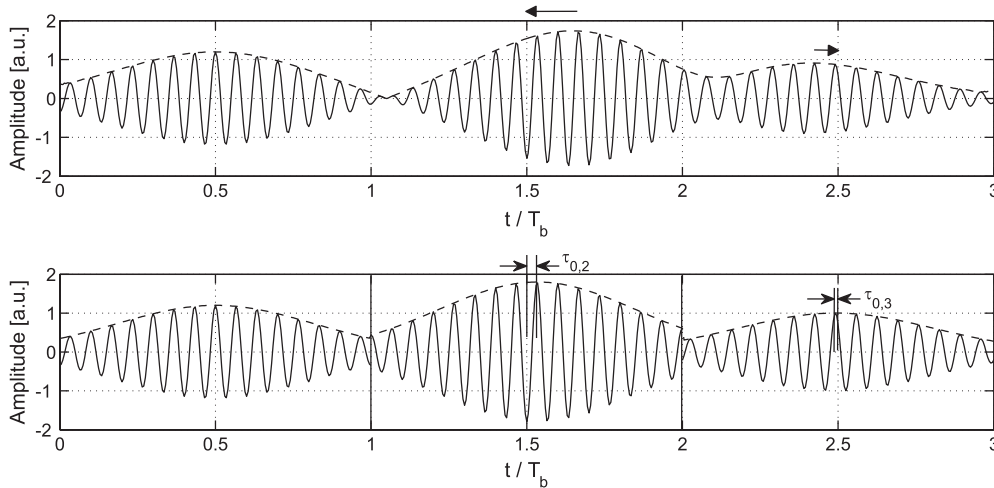


Figure 3. Top: three consecutive Doppler bursts with random arrival times $t_{0,i}$. Bottom: simplified model where overlaps between consecutive bursts are neglected but their random phases are maintained via the time offsets $\tau_{0,i}$. The dashed lines mark the signal envelopes. Note that only the undisturbed signal is shown for $T_b/T_w = 0.9$.

of single scattering particles with random amplitude \hat{A}_i that are appearing at random times $t_{0,i}$ (see figure 2, bottom). These burst signals $m_{s,i}$ originate from dominant speckles or scattering centers on the object surface, which are passing the measurement volume successively. Due to the constant object velocity v_x and the fixed shape of the interference fringe system over time, the Doppler frequency f_D and the parameter $w = N_{\text{fringes}}/2$ are equal for all individual Doppler bursts $m_{s,i}$ (cf figure 2). This means that all burst signals $m_{s,i}$ are of equal duration $T_w = 2w_t = 2w/f_D$. Consequently, the following model equation results for the undisturbed and high-pass-filtered scattered light signal of a moving rough solid surface:

$$\begin{aligned} m[k] &= \sum_{i=1}^M m_{s,i}[k] \\ &= \sum_{i=1}^M \hat{A}_i e^{-\frac{2f_D^2(k/f_s - t_{0,i})^2}{w^2}} \cos(2\pi f_D(k/f_s - t_{0,i})), \\ k &= 0, \dots, N. \end{aligned} \quad (7)$$

This model does not include the low-frequency part, i.e. the slowly varying offset of the originally detected signal (cf figure 2, top). However, this is acceptable since this slowly varying offset contains no information about the Doppler frequency f_D and can be neglected accordingly. In particular, the low-frequency part of the bursts $m_{s,i}$, which is included in this offset, does not influence the CRLB for the Doppler frequency estimation (see appendix A.1) because the noise contained in the detected signal can be assumed to be signal independent by approximation (see subsection 2.3).

In order to be able to calculate the CRLB analytically, one further simplification has to be introduced to the model represented by equation (7). The overlap between consecutive burst signals is random and, thus, it is difficult to model analytically. However, the average overlap at both edges of the burst signal together amounts to only about 10–20% of the $1/e^2$ burst width in practice corresponding

to a relation of $T_b/T_w = 0.8\text{--}0.9$, where $T_w = 2w_t$ is the constant $1/e^2$ burst width and T_b denotes the average time interval between two successive bursts in the scattered light signal. This holds in fact for scattered light signals from objects with different surface characteristics. In addition, these overlaps occur at the edges of the burst signals where the signal amplitudes are much lower than in the center of the bursts (cf figure 2). Thus it can be assumed that the amount of energy superimposed from neighboring bursts is small compared to the energy of the respective burst signal itself. Therefore, the influence of the overlapping signal parts from adjacent bursts on the Doppler frequency estimation will be relatively small. Consequently, the overlap from neighboring burst signals can be neglected in an initial approximation. However, the random phase shifts between the harmonic Doppler oscillations of successive burst signals must not be neglected. Otherwise, all burst signals would have a fixed phase relationship, which is not true. According to these considerations, we simplify our model by assuming that the consecutive Doppler bursts $m_{s,i}$ appear at constant time intervals T_b , whereupon T_b is defined as the average time interval between two successive bursts in the actual detected scattered light signal. Thereby, overlaps between consecutive bursts $m_{s,i}$ are neglected. Essentially this means that the bursts are shifted imaginarily in time to the center of consecutive time intervals of equal width T_b as shown in figure 3. Thus, their original arrival times $t_{0,i}$ are replaced by

$$\tilde{t}_{0,i} = \left(i - \frac{1}{2}\right) T_b + \tau_{0,i}, \quad i = 1, \dots, M. \quad (8)$$

The parameter $\tau_{0,i}$ denotes a tiny random time offset that shifts the individual bursts slightly away from the center of the time intervals of width T_b (see figure 3). This is to maintain the random phase of the consecutive Doppler bursts which is uniformly distributed within the interval $[-\pi; \pi]$. Consequently, subsequent bursts exhibit a random phase shift with respect to the Doppler modulation. In contrast to the original signal where a gradual phase transition occurred

between successive bursts (see figure 3, top), the phase shifts happen abruptly in the simplified model (see figure 3, bottom). However, the effect of ending up with incoherent signal sections is the same. As a result, the analytical model of the undisturbed signal of equation (7) simplifies to

$$m[k] \approx m_{s,i}[k] = \hat{A}_i e^{-\frac{2f_D^2(k/f_s - \tilde{t}_{0,i})^2}{w^2}} \cos(2\pi f_D(k/f_s - \tilde{t}_{0,i}))$$

with $i = \left\lceil \frac{k}{N_0} \right\rceil$ and $k = 0, \dots, (N-1)$ and $N = N_0 M$ (9)

representing a chain of M equidistant Doppler bursts $m_{s,i}$ each with a duration $T_b = N_0/f_s$ corresponding to a length of N_0 samples and with random amplitude and phase (cf figure 3). This simplified signal model is a fundamental prerequisite that enables calculating the CRLB analytically, and it is used exclusively for this purpose. Neglecting the overlap of consecutive bursts seems to be acceptable since numerically simulated Doppler spectra using equation (9) coincide very well with the spectra of measured scattered light signals. Also the results presented in section 4 confirm the permissibility of this simplification. Nevertheless, it should be investigated in future if or how the requirement for this simplification can be lifted.

In summary, the following assumptions and simplifications have been made for deriving the analytical model in equation (9) for the undisturbed scattered light signal of a moving rough solid surface.

- The interference fringe spacing d is assumed to be constant neglecting the effect of fringe spacing variations.
- The object is passing through the measurement volume perpendicular to the interference fringes with constant velocity v_x (acceleration is not considered here).
- The low-frequency part of the signal without any Doppler modulation is neglected since the noise can be assumed to be signal independent (see subsection 2.3).
- The successive Doppler bursts $m_{s,i}$ exhibit equal Doppler frequency f_D and equal duration $T_w = 2w_t = 2w/f_D$ ($w = \text{constant}$) but random amplitude \hat{A}_i and random phase uniformly distributed within the interval $[-\pi; \pi]$.
- At the signal model, imaginary, the bursts are equally spaced at time intervals T_b and the overlap between consecutive bursts is neglected (see figure 3, bottom).
- The individual bursts are located approximately in the center of the corresponding time intervals of length T_b according to equation (8).

The $2M+2$ unknown parameters of this signal model $m[k]$ are the Doppler frequency f_D , the constant parameter w , the amplitudes of the M successive Doppler bursts $\hat{A}_1, \dots, \hat{A}_M$ and their individual arrival times $\tilde{t}_{0,1}, \dots, \tilde{t}_{0,M}$ that include implicitly the random and unknown phase shifts between the consecutive burst signals. These unknown parameters can be summarized in the vector

$$\vec{a} = (f_D, \hat{A}_1, \dots, \hat{A}_M, w, \tilde{t}_{0,1}, \dots, \tilde{t}_{0,M})^T. \quad (10)$$

2.3. Noise

The measured scattered light signals always contain noise which can be generally divided into two categories. On the one hand, there is signal-independent noise which mainly corresponds to thermal noise from the photodetector and the subsequent electronics. It can be described in good approximation by a Gaussian distribution [20]. On the other hand, also signal-dependent shot noise is generated both optically at the photon emission inside monochromatic laser light sources and electrically during photodetection, which follows a Poisson distribution. However, the offset in the scattered light signals of moving rough solid surfaces is large compared to the amplitude of the Doppler modulation. In addition, this offset varies only slightly and slowly over time as long as the object surface characteristics do not change significantly (see figure 2, top). This is generally fulfilled in good approximation within the finite time duration of a short signal segment used for determining one individual Doppler frequency breakpoint, because the object surface moves only a short way within this finite time duration. Furthermore, abrupt changes in the surface characteristics are relatively unlikely to occur. Thus, the resulting shot noise power can be assumed to be approximately constant over time. Moreover, the large average signal amplitude (offset) causes a large shot noise level resulting in a large mean of the corresponding Poisson distribution. In this case, the Poisson distribution can be approximated by a Gaussian distribution [20]. Consequently, the noise can be regarded in total as approximately time independent, and it can be described collectively by a Gaussian distribution with constant variance σ_n^2 . Moreover, the consecutive samples of the scattered light signal $\vec{x} = (x[0], x[1], \dots, x[N-1])^T$ can be assumed to be stochastically independent as long as the sampling frequency f_s does not exceed twice the noise bandwidth. As a result, the following joint probability density function is obtained:

$$p(\vec{x}, \vec{a}) = \prod_{k=0}^{N-1} \frac{1}{\sqrt{2\pi\sigma_n^2}} e^{-\frac{(x[k]-m[k])^2}{2\sigma_n^2}}$$

$$= \left(\frac{1}{2\pi\sigma_n^2}\right)^{\frac{N}{2}} e^{-\frac{1}{2\sigma_n^2} \sum_{k=0}^{N-1} (x[k]-m[k])^2} \quad (11)$$

with $N = N_0 M$. This includes white noise assumption and a detector bandwidth equaling the Nyquist frequency $f_s/2$. Considering only a single Doppler burst $m_{s,i}$, $i = 1, \dots, M$, with sample length N_0 , the joint probability density function of the corresponding signal $\vec{x}_i = (x_i[0], x_i[1], \dots, x_i[N_0-1])^T$ is

$$p(\vec{x}_i, \vec{a}_{s,i}) = \left(\frac{1}{2\pi\sigma_n^2}\right)^{\frac{N_0}{2}} e^{-\frac{1}{2\sigma_n^2} \sum_{k=0}^{N_0-1} (x_i[k]-m_{s,i}[k])^2}. \quad (12)$$

3. CRLB calculation

3.1. Approach

For the general approach, first, the regularity condition

$$E \left\{ \frac{\partial \ln p(\vec{x}, \vec{a})}{\partial a_j} \right\} = 0, \quad j \in \{1, 2, \dots, 2M+2\}, \quad \forall \vec{a}, \quad (13)$$

must be checked to be fulfilled. For Gaussian joint probability density functions such as described by equations (11) and (12), this is always true as proven in [18, 21]. Then the Fisher information matrix \mathbf{I} must be calculated. Its elements are given by

$$\mathbf{I}_{hj} = -E \left\{ \frac{\partial^2 \ln p(\vec{x}, \vec{a})}{\partial a_h \partial a_j} \right\}, \quad h, j \in \{1, 2, \dots, 2M + 2\}. \quad (14)$$

Finally, the CRLB is defined as the inverse of the Fisher information $I(f_D)$. In case of the Doppler frequency estimation, it equals the first diagonal element of the inverse \mathbf{I}^{-1} of the Fisher information matrix satisfying the condition

$$\text{var}(\hat{f}_D) \geq \text{CRLB}(\hat{f}_D) = \frac{1}{I(f_D)} = [\mathbf{I}^{-1}]_{11}. \quad (15)$$

This means that the variance of any unbiased estimator \hat{f}_D for the Doppler frequency f_D is larger than or equal to the CRLB. Hence, the CRLB represents the minimum achievable uncertainty of the Doppler frequency estimation.

To facilitate the derivation of the CRLB for the Doppler frequency estimation from scattered light signals of moving rough solid surfaces, we are utilizing the additive nature of the Fisher information [21]. According to equation (9), we neglected the overlap between successive Doppler bursts $m_{s,i}$, $i = 1, \dots, M$, in our signal model. In addition, the consecutive samples of the scattered light signal \vec{x} can be assumed to be stochastically independent (see section 2.3). Consequently, the individual bursts $m_{s,i}$ are stochastically independent too. Thus, the total Fisher information $I(f_D)$ about the Doppler frequency f_D equals the sum of information gathered from observing these stochastically independent bursts $m_{s,i}$ individually, which can be expressed mathematically by

$$I(f_D) = \sum_{i=1}^M I_{s,i}(f_D). \quad (16)$$

Hence, equation (15) can be rewritten resulting in the following relation for the CRLB:

$$\text{var}(\hat{f}_D) \geq \text{CRLB}(\hat{f}_D) = \frac{1}{\sum_{i=1}^M I_{s,i}(f_D)}. \quad (17)$$

Since $I_{s,i}(f_D) = 1/\text{CRLB}_{s,i}(\hat{f}_D)$, the calculation of the CRLB for the Doppler frequency estimation from the scattered light signal of a moving rough solid surface, which is modeled as a chain of M single Doppler bursts $m_{s,i}$ according to equation (9), can be broken down to determine the respective CRLB for these individual burst signals $\text{CRLB}_{s,i}(\hat{f}_D)$.

3.2. Generalized analytical expression for a single burst signal

According to equation (17), it is necessary to derive an analytical expression for $\text{CRLB}_s(\hat{f}_D) = 1/I_s(f_D)$ denoting the CRLB for the frequency estimation from a single burst signal modeled by equation (5) for signal-independent Gaussian white noise.

In previous works, several analytical expressions for this CRLB have been derived under different assumptions. After

the scattered light signal has been modeled as a harmonic function in early works [14], Besson *et al* first calculated a CRLB corresponding to the model of equation (5) also taking into account the Gaussian signal envelope [15]. However, the width of the Gaussian envelope was considered to be a known parameter which is not appropriate in general (cf appendix A.2). Later on, Shu [16] and Sobolev *et al* [17] carried out similar calculations to Besson *et al*'s by applying a signal model comprising two harmonic signals with a $\pi/2$ phase shift. Such a signal pair can be obtained using a carrier frequency and mixing down the burst signal to the baseband in quadrature manner. However, the noises of both signals were considered to be stochastically independent of each other which is not true in general, e.g. for noise due to photodetection. In [18] these constraints and limitations have been overcome, but the signal duration T_b was assumed to be large compared to the Gaussian envelope width $T_w = 2w_t = 2w/f_D$ corresponding to $T_b \rightarrow \infty$. Since the average burst duration T_b within a scattered light signal of a moving rough solid surface varies as a function of the surface characteristics and is of similar size as the Gaussian envelope width T_w of the individual bursts (cf section 2.2), this simplification is also not acceptable here. Therefore, we calculated the CRLB without this simplification.

Inserting the signal model of equation (5) together with the vector of unknown parameters (see equation (6)) into the general approach described in the previous subsection, the following generalized analytical expression results for the CRLB of the Doppler frequency estimation from a single burst signal (see appendix A.1):

$$\begin{aligned} \text{CRLB}_s(\hat{f}_D) &= \frac{64\sigma_n^2}{\sqrt{\pi}\pi^2 f_s \hat{A}^2 T_w^3 c_2(\eta)} \\ &= \frac{64}{\sqrt{\pi}\pi^2 c_2(\eta)} \cdot \frac{\sigma_n^2}{f_s} \cdot \frac{1}{\hat{A}^2 N_{\text{fringes}}^3} \cdot f_D^3 \quad (18a) \\ &= \frac{8c(\eta)}{\pi^2 N_0 T_w^2 \text{SNR}_s} \quad (18b) \end{aligned}$$

with

$$\begin{aligned} T_w &= \frac{2w}{f_D} = \frac{N_{\text{fringes}}}{f_D} \\ \eta &= \frac{T_b}{T_w} = \frac{N_0}{f_s T_w} \\ c_2(\eta) &= \text{erf}(2\eta) - \frac{4\eta}{\sqrt{\pi}} e^{-4\eta^2} \\ c(\eta) &= \frac{\text{erf}(2\eta)}{c_2(\eta)} = \frac{\text{erf}(2\eta)}{\text{erf}(2\eta) - \frac{4\eta}{\sqrt{\pi}} e^{-4\eta^2}} \\ \text{SNR}_s &= \frac{P_s}{\sigma_n^2} \approx \frac{\frac{\sqrt{\pi}\hat{A}^2}{8\eta} \text{erf}(2\eta)}{\sigma_n^2}. \end{aligned}$$

This universal result is consistent and in accordance with previously derived CRLB formulas as verified in appendix A.3. It can be expressed in two different ways: one is equation (18a) that shows the fundamental dependencies of the CRLB for the Doppler frequency estimation from a single burst signal on the

signal amplitude \hat{A} , the noise power spectral density σ_n^2/f_s , the number of interference fringes N_{fringes} , and the Doppler frequency f_D itself. For practical considerations, an expression in terms of signal parameters such as the number of samples N_0 , the temporal burst width T_w and the signal-to-noise ratio SNR_s defining the ratio between the average burst signal power \bar{P}_s and the noise power σ_n^2 is often more convenient. Hence, equation (18b) is given alternatively which reveals that the minimum achievable uncertainty of the Doppler frequency estimation decreases for a single burst signal with increasing SNR_s , with increasing temporal $1/e^2$ burst width T_w , and with increasing number of acquired samples N_0 . The parameter η defines the ratio between the burst signal duration T_b and the $1/e^2$ width of the Gaussian burst envelope T_w . Consequently, $c_2(\eta)$ and $c(\eta)$ converge to 1 when the signal duration is large compared to the burst width ($T_b \gg T_w$) corresponding to $\eta \rightarrow \infty$. Already for $\eta \geq 1.15$, $c_2(\eta) > 0.99$ and $c(\eta) < 1.01$. However, for small values of η corresponding to $T_b \leq T_w$, the parameters $c_2(\eta)$ and $c(\eta)$ effect a significant increase of the $\text{CRLB}_s(\hat{f}_D)$.

3.3. Analytical result for scattered light signals from moving rough surfaces

For determining the CRLB of the Doppler frequency estimation for scattered light signals from moving rough surfaces, equation (18a) has to be inserted into equation (17) with $I_{s,i}(f_D) = 1/\text{CRLB}_{s,i}(\hat{f}_D)$:

$$\begin{aligned} \text{CRLB}(\hat{f}_D) &= \frac{1}{\sum_{i=1}^M \frac{1}{\text{CRLB}_{s,i}(\hat{f}_D)}} \\ &= \frac{64}{\sqrt{\pi} \pi^2 c_2(\eta)} \cdot \frac{\sigma_n^2 f_D^3}{f_s N_{\text{fringes}}^3 M \frac{1}{M} \sum_{i=1}^M \hat{A}_i^2}. \end{aligned} \quad (19)$$

Using the mean square burst amplitude $\overline{\hat{A}^2} = \frac{1}{M} \sum_{i=1}^M \hat{A}_i^2$ and the relation for the signal duration

$$T = M T_b = M \eta T_w = \frac{M \eta N_{\text{fringes}}}{f_D}, \quad (20)$$

the following result is obtained:

$$\begin{aligned} \text{var}(\hat{f}_D) \geq \text{CRLB}(\hat{f}_D) &= \frac{64 \eta}{\sqrt{\pi} \pi^2 c_2(\eta)} \\ &\cdot \frac{\sigma_n^2}{f_s} \cdot \frac{1}{\overline{\hat{A}^2} N_{\text{fringes}}^2 T} \cdot f_D^2 \quad (21a) \\ &= \frac{8 c(\eta)}{\pi^2 N T_w^2 \text{SNR}} \quad (21b) \end{aligned}$$

with

$$N = N_0 M = f_s T \quad \text{and} \quad \text{SNR} = \frac{\bar{P}}{\sigma_n^2} = \frac{\sqrt{\pi} \overline{\hat{A}^2}}{8 \eta \sigma_n^2} \text{erf}(2\eta).$$

Equations (21a) and (21b) provide for the first time a simple analytical expression for calculating the minimum achievable uncertainty of the Doppler frequency estimation for scattered light signals from moving rough solid surfaces. Again, two different expressions are given: equation (21a) shows the

fundamental dependences on the noise power spectral density σ_n^2/f_s , the mean square burst amplitude $\overline{\hat{A}^2}$, the number of interference fringes N_{fringes} , the signal duration T , and the Doppler frequency f_D . Alternatively, equation (21b) can be used for practical uncertainty estimations. It shows that the minimum attainable uncertainty of the Doppler frequency estimation decreases with increasing signal-to-noise ratio (SNR), i.e. with increasing average signal power \bar{P} or mean square burst amplitude $\overline{\hat{A}^2}$, respectively, with increasing temporal $1/e^2$ burst width T_w , with increasing number of totally acquired samples $N = f_s T$, i.e. with increasing signal length, and with increasing time interval between consecutive bursts T_b relative to T_w expressed by the parameter η .

Interestingly, if we assume a noisy single-tone signal $s[k] = A \cos(2\pi f k/f_s)$ with constant amplitude A but equal SNR, the resulting well-known CRLB (see [2], equation (6.84) on page 298)

$$\text{var}(\hat{f}) \geq \text{CRLB}_{\text{single-tone}}(\hat{f}) \approx \frac{3 f_s^2}{\pi^2 N^3 \text{SNR}} = \frac{3}{\pi^2 N T^2 \text{SNR}} \quad (22)$$

exhibits the same structure as equation (21b) apart from a constant factor $8c(\eta)/3$. However, the essential difference is that the lower bound of equation (22) decreases with the third power of the signal length $\sim 1/N^3$, whereas equation (21b) decreases only linearly with increasing signal length $\sim 1/N$ since it depends on the constant burst width T_w instead of the total signal duration T . This is due to the fact that consecutive Doppler bursts of a scattered light signal of a moving rough solid surface have to be treated as independent and non-coherent signal parts due to their random phase (see section 2.2), which is not considered in equation (22). Thus, the frequency estimation uncertainty is significantly higher for a scattered light signal of a moving rough solid surface with non-coherent signal parts (Doppler bursts) than for a coherent noisy single-tone signal where all signal parts are in phase.

4. Comparison with experimental results

In order to demonstrate the validity of the analytical result of equations (21a) and (21b), a comparison with experimental data was made. For this purpose, measurement data sets have been used that originate from experimental investigations carried out independently of and previously to the theoretical work presented in this paper. The employed laser Doppler sensor setup is described in [9]. In contrast to [9], the front lens of the sensor head had been exchanged resulting in interference fringe systems that exhibited a length of 1.5 mm and a lateral width of 0.1 mm. The average interference fringe spacing d amounted to about $7 \mu\text{m}$ in the middle of the measurement volume. For the investigations described in this section, the scattered light signals of only one interference fringe system have been evaluated. The axial position z , where the test object surface passed the interference fringes, has been the same for all measurements considered here. As a test object, a planar piece of aluminum sheet exhibiting an arithmetical mean surface roughness index $R_a = 0.2 \mu\text{m}$ has been used, which was moved laterally through the

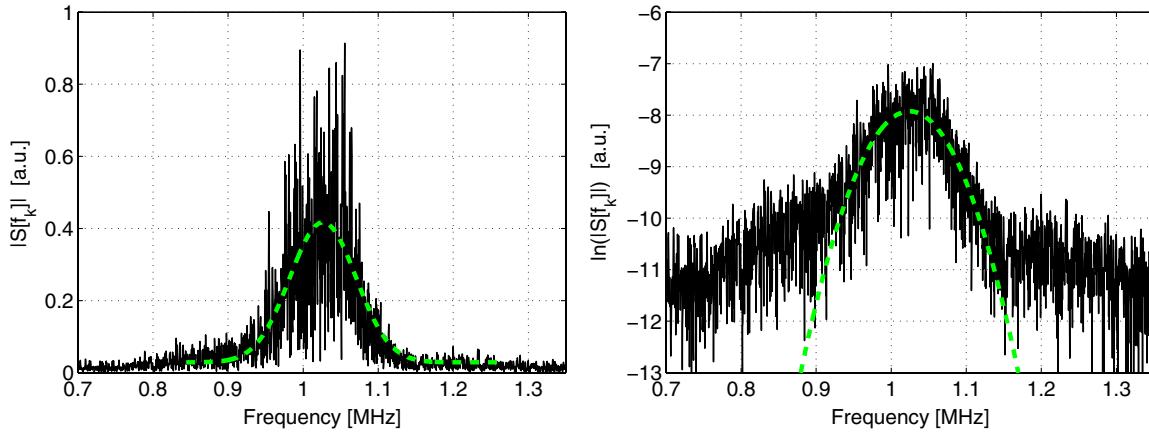


Figure 4. Left: amplitude spectrum of a detected and high-pass-filtered scattered light signal of a rough solid surface together with a Gaussian regression curve (dashed line). Right: corresponding logarithmic spectrum with parabolic regression curve (dashed line).

interference fringes with a constant velocity $v_x = 6.9 \text{ m s}^{-1}$. The resulting Doppler frequency f_D was estimated by evaluating the detected scattered light signal using different signal processing techniques, which are described in the following subsection 4.1. Via repeated measurements, the relative standard deviations σ_{f_D}/f_D of the estimated Doppler frequencies were determined and compared to the derived CRLB in section 4.2.

4.1. Signal processing techniques for Doppler frequency estimation

Several different techniques for Doppler frequency estimation based on counting procedures, correlation techniques, analog and digital spectral analysis or quadrature demodulation methods are known [2]. Many of these techniques were developed for evaluating burst signals of single scattering particles in fluid flows. For application to scattered light signals of rough solid surfaces exhibiting random amplitude fluctuations and phase jumps (see section 2.2), extended and more sophisticated methods are required. For our study, we used four different signal processing techniques for Doppler frequency estimation, which are briefly described in the following.

The first two techniques are based on digital spectral analysis employing a fast Fourier transform (FFT) to calculate the spectrum of the detected and high-pass-filtered scattered light signals. The one-sided spectrum $S[f_k]$ of the signal $m[k]$ according to equation (7) or (9), respectively, can be written as

$$S[f_k] = \sqrt{\frac{\pi}{2}} \frac{w}{f_D} e^{-\frac{\pi^2 w^2}{4f_D^2} (f_k - f_D)^2} \cdot \sum_{i=1}^M \hat{A}_i e^{-j2\pi f_k t_{0,i}} + N[f_k]$$

with $f_k = kf_s/N$ and $k = 0, \dots, \frac{N}{2} - 1$. (23)

$N[f_k]$ denotes the spectrum of the superposed noise. Because of the invariance of the Gaussian function with the Fourier transform, the spectral peak at the Doppler frequency f_D again exhibits a Gaussian shape. However, this Gaussian peak is severely distorted (see figure 4, left) due to the sum term

in equation (23) which results from the random amplitude fluctuations and phase jumps in the time domain scattered light signal caused by speckles [7]. These distortions are concealing the center frequency of the Gaussian peak that is equal to the Doppler frequency f_D . Thus, in method one named ‘FFT + Gaussian curve fit’, a Gaussian regression curve is fitted to the spectral Doppler peak via an iterative least-squares algorithm to determine f_D (see figure 4, left). The main drawback of this method is that the necessary iterative curve fit is time consuming.

Therefore, a second method called ‘ln(FFT) + parabolic curve fit’ employs the natural logarithm of the spectrum described by equation (23) exhibiting a parabolic shape except for the approximately constant noise floor $\ln(|N[f_k]|)$. Thus a parabolic curve fit can be used to determine the Doppler frequency (see figure 4, right), which is much faster than the iterative Gaussian fit of method one since it can be calculated analytically. However, the fitting region has to be well confined to the Doppler peak in order to minimize the influence of the noise floor $\ln(|N[f_k]|)$, for which reason some part of the available information is lost.

The third method working in time domain employs a quadrature demodulation technique (QDT) [22], where the complex analytical signal

$$m^*[k] = m[k] + j\mathcal{H}\{m[k]\} \quad (24)$$

is evaluated, which can be generated using the Hilbert transform \mathcal{H} . If $m[k]$ is a harmonic function, the momentary signal frequency $f[k]$ equals the derivative of the phase $\varphi[k]$ with respect to time according to

$$f[k] = \frac{\varphi[k] - \varphi[k-1]}{2\pi f_s} \quad \text{with} \quad \varphi[k] = \arg\{m^*[k]\}$$

$$= \arctan \left\{ \frac{\mathcal{H}\{m[k]\}}{m[k]} \right\}. \quad (25)$$

Finally, the sought after Doppler frequency is obtained as the weighted average of $f[k]$. However, for a correct and precise Doppler frequency determination, it is crucial to apply an appropriate weighting function and to eliminate the phase jumps between consecutive signal bursts reliably. This is very difficult and laborious.

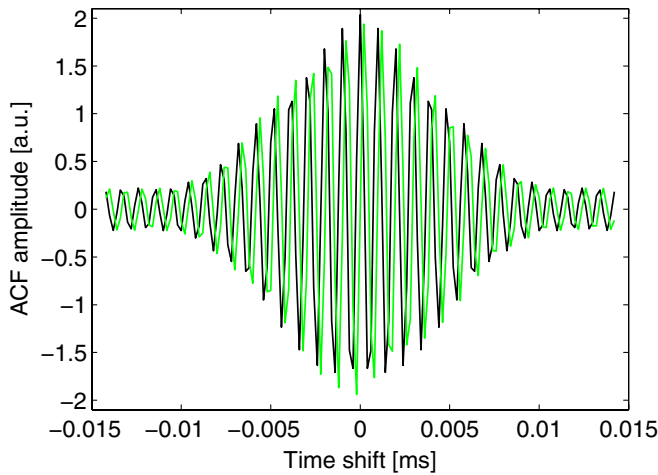


Figure 5. Central region of the autocorrelation function (ACF) of a detected and high-pass-filtered scattered light signal of a rough solid surface together with the corresponding Hilbert transform (light green curve) representing a 90° phase-shifted signal version.

For this reason, a fourth method named ‘ACF + QDT’ was invented. It applies the QDT not to the scattered light signal itself but to its autocorrelation function (ACF). The advantage of using the ACF is that the central region of the ACF shown in figure 5 exhibits no phase jumps and almost no noise apart from the very center, where the white noise is concentrated. Thus, a few signal points around zero time shift have to be excluded from evaluation. Except for that, the QDT algorithm described before can be applied very easily to the central region of the ACF enabling a relatively quick and robust Doppler frequency estimation.

4.2. Comparison

To validate equations (21a) and (21b), respectively, scattered light signals of the moving rough test object surface were recorded at a sampling frequency of $f_s = 5$ MHz and evaluated using the signal processing techniques described above. The Doppler frequency amounted to $f_D = 1.01$ MHz on average (cf figure 4). The signal length, i.e. the number of acquired samples per signal, was varied within the interval $N = 76 \dots 9000$, for which the minimum length of $N = 76$ samples corresponds to the $1/e^2$ width $T_w = 76/f_s = 2w/f_D = 15 \mu s$ of a single Doppler burst. For each of the selected signal lengths, 180 repeated measurements were carried out under the same conditions and for the same region on the test object for calculating the respective relative standard deviations σ_{f_D}/f_D of the estimated Doppler frequencies. The relative average time interval between consecutive bursts was determined from the measured scattered light signals to be $\eta = T_b/T_w = 0.816$ resulting in $c(\eta = 0.816) = 1.08$. The average SNR of the detected scattered light signals varied for the different selected signal lengths between 13.8 and 15.4 dB. By transforming equation (21b) according to

$$\frac{\sigma_{f_D}}{f_D} \geq \frac{\sqrt{8c(\eta)}}{\pi T_w f_D \sqrt{N} \sqrt{\text{SNR}}} \quad (26)$$

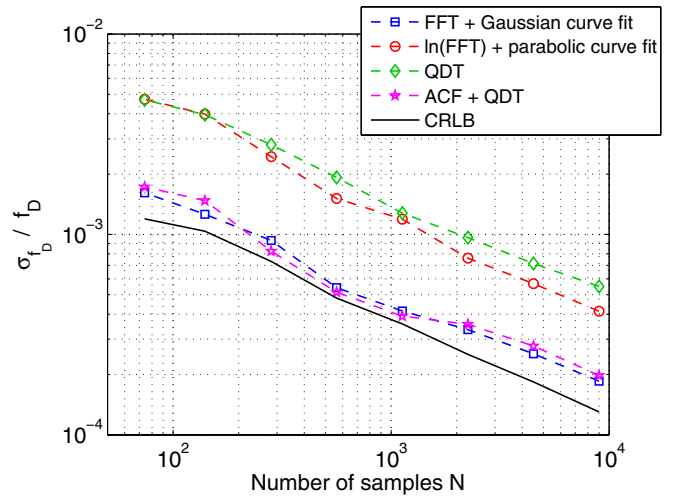


Figure 6. Relative standard uncertainty σ_{f_D}/f_D of the Doppler frequency estimation as a function of the length N of the detected and digitalized scattered light signals of a moving rough test object experimentally obtained using four different signal processing techniques described in section 4.1 in comparison with the calculated CRLB.

and inserting the above values into this equation, the CRLB for the relative standard uncertainty of the Doppler frequency estimation σ_{f_D}/f_D was calculated for each case, and it was compared to the experimentally obtained results using the four different signal processing techniques described in section 4.1. The results of this comparison are shown in figure 6.

According to equation (26), σ_{f_D}/f_D decreases with $1/\sqrt{N}$. The CRLB curve in figure 6 deviates slightly from this $1/\sqrt{N}$ -dependence, because the CRLB is also influenced by the SNR which was not precisely constant but varied a little from one test series to the next (see above as well as equation (26)). Nevertheless, all four measurement curves follow this dependence approximately and decrease with about $1/\sqrt{N}$. In particular, the measurement results for the signal processing methods ‘FFT + Gaussian curve fit’ and ‘ACF + QDT’ follow the CRLB curve very closely. On average, the outcomes of both methods are only by a factor of 1.3 larger than the calculated CRLB according to equation (26) indicating high efficiency of these methods (see figure 6). For the methods ‘ln(FFT) + parabolic curve fit’ and ‘QDT’, the obtained relative standard uncertainties σ_{f_D}/f_D are farther away from the CRLB with differences amounting to factors of 3.4 and 3.9, respectively. In the case of the method ‘ln(FFT) + parabolic curve fit’, the higher uncertainty is due to the fact that some part of the information contained in the spectrum cannot be used for estimating the Doppler frequency f_D via the parabolic fit because of the distracting noise floor (see section 4.1). In the ‘QDT’ method, it is hardly possible to eliminate reliably all the phase jumps occurring between consecutive signal bursts which results in disturbances for the Doppler frequency estimation.

Altogether, the obtained experimental results agree very well with the derived analytical CRLB according to equations (21a), (21b) and (26), which defines the theoretical lower limit for the achievable uncertainty of the Doppler

frequency estimation for scattered light signals of rough solid surfaces for any unbiased estimator. This also holds for test results obtained at different object velocities, at different SNR, and with other surfaces exhibiting different mean surface roughness indices, respectively, which are not shown here for reason of conciseness. In particular, the excellent conformity with the determined relative standard uncertainties σ_{f_D}/f_D using the signal processing methods ‘FFT + Gaussian curve fit’ and ‘ACF + QDT’ substantiates the validity and the correctness of the derived analytical CRLB result (see figure 6).

5. Implications for laser Doppler measurements on moving rough surfaces

Both for conventional LDV sensors and for extended laser Doppler techniques such as the LDDS, which is able to measure the axial position z of moving rough object surfaces in addition to its transverse velocity v_x , the relative standard uncertainty σ_{v_x}/v_x of the velocity measurement depends directly on the relative standard uncertainty of the Doppler frequency estimation σ_{f_D}/f_D (see equations (1) and (2)). Using equation (21a), the CRLB for σ_{f_D}/f_D can be expressed analytically by

$$\frac{\sigma_{f_D}}{f_D} \geq \frac{8\sqrt{\eta}}{\pi^{5/4}\sqrt{c_2(\eta)}} \cdot \sqrt{\frac{\sigma_n^2}{f_s} \cdot \frac{1}{\hat{A}^2 N_{\text{fringes}}^2 T}} \quad (27)$$

Consequently, the minimum attainable relative standard uncertainty of the velocity measurement σ_{v_x}/v_x of laser Doppler methods on rough moving surfaces decreases with decreasing noise power spectral density σ_n^2/f_s , with increasing mean square burst amplitude \hat{A}^2 , i.e. with increasing signal power, with increasing number of interference fringes N_{fringes} , and with increasing signal duration T . It is important to note that the noise power spectral density σ_n^2/f_s is constant for a given detector and cannot be influenced by varying the sampling rate f_s . The parameter η is normally around 1. Thus, also $c_2(\eta)$ has no significant influence as long as η does not fall considerably below 1 (cf section 3.2).

In the case of the LDDS, the axial object position z is measured as well [6, 7]. Aside from a calibration factor s , the position standard uncertainty σ_z depends on the relative standard uncertainty of the Doppler frequency estimation σ_{f_D}/f_D too (see equation (2)). Here, approximately equal Doppler frequencies $f_{D1} \approx f_{D2} \approx f_D$ and frequency uncertainties $\sigma_{f_{D1}} \approx \sigma_{f_{D2}} \approx \sigma_{f_D}$ are assumed for the two measuring channels of the LDDS which is fulfilled in good approximation in practice [6, 7]. For position and distance measurements, the lateral resolution Δx is of particular interest which is equal to the lateral averaging length on moving object surfaces. Hence, the CRLB of the position estimation is expressed in terms of Δx by inserting the relations

$$T = \frac{\Delta x}{v_x} = \frac{\Delta x}{f_D d} \quad \text{and} \quad N_{\text{fringes}} = \frac{2w_x}{d}, \quad (28)$$

as well as equation (27) into equation (2). As a result, we obtain

$$\sigma_z \geq \frac{8\sqrt{2\eta}}{s \pi^{5/4}\sqrt{c_2(\eta)}} \cdot \sqrt{\frac{\sigma_n^2}{f_s} \cdot \frac{f_D d^3}{\hat{A}^2 (2w_x)^2 \Delta x}}, \quad (29)$$

in which $2w_x$ denotes the lateral width of the measurement volume, i.e. of the two superposed interference fringe systems (cf section 2.1). The parameter d identifies the average fringe spacing. For a given sensor setup, the parameters s , d and $2w_x$ are constant. Generally, the parameter $c_2(\eta) \approx 1$ since usually $\eta \approx 1$. The Doppler frequency f_D depends on the lateral object velocity. Consequently, the minimum attainable standard uncertainty σ_z of the position estimation of the LDDS on rough moving surfaces can be decreased mainly by decreasing the noise power spectral density σ_n^2/f_s via the use of a low-noise detector, by increasing the signal power corresponding to \hat{A}^2 , and by increasing the lateral averaging length on the object surface Δx (see equation (29)). The latter constitutes an uncertainty relation between lateral resolution Δx and axial position resolution σ_z .

For comparison with experimental data, it is again advantageous to rewrite equation (29) in terms of the SNR according to

$$\sigma_z \geq \frac{4\sqrt{c(\eta)}}{s \pi} \cdot \sqrt{\frac{f_D}{f_s} \cdot \frac{d^3}{\text{SNR} (2w_x)^2 \Delta x}}, \quad (30)$$

which does not change the dependence of σ_z on $1/\sqrt{\Delta x}$. To validate equations (29) and (30), test measurements have been carried out using the same test object as for the experiments described in section 4. The employed LDDS exhibited the following design parameters: $s = 0.36 \text{ mm}^{-1}$, $d \approx 6.97 \text{ }\mu\text{m}$ and $2w_x = 105 \text{ }\mu\text{m}$. The test object surface was moved laterally along the x -axis through the measurement volume of the LDDS at a fixed position z and with a constant velocity $v_x = 6.9 \text{ m s}^{-1}$. The measured Doppler frequencies amounted to about 1 MHz at a sampling frequency of $f_s = 5 \text{ MHz}$. The detected scattered light signals exhibited an SNR of about 14.5 dB and the parameter η was determined to be $\eta = 0.82$ resulting in $c(\eta) = 1.08$. At different lateral averaging lengths Δx , 30 repeated measurements were carried out in each case at a constant object position z . From the measured positions, the standard deviations σ_z were calculated and compared to the CRLB according to equation (30). The results are shown in figure 7. The experimental results are in very good agreement with the analytically derived CRLB. On average, the measured position uncertainties are larger than the CRLB only by a factor of 1.32, which demonstrates the efficiency of the signal processing algorithms used for position estimation. On the other hand, this excellent agreement between experimental results and theory underlines the validity of the derived analytical relations of equations (21a), (21b) and (30). Besides, these measurement results confirm the uncertainty relation between the lateral resolution Δx and the axial position resolution σ_z . In the LDDS setup used, a standard position uncertainty $\sigma_z < 2 \text{ }\mu\text{m}$ is obtained for averaging lengths $\Delta x > 0.65 \text{ mm}$ (see figure 7).

Consequently, the derived analytical CRLB expression of equations (21a) and (21b) allows not only an easy estimation of the minimum attainable measurement uncertainties of laser Doppler sensors on moving rough solid surfaces for the first time, it also shows directly the influences of certain system and signal parameters on these measurement

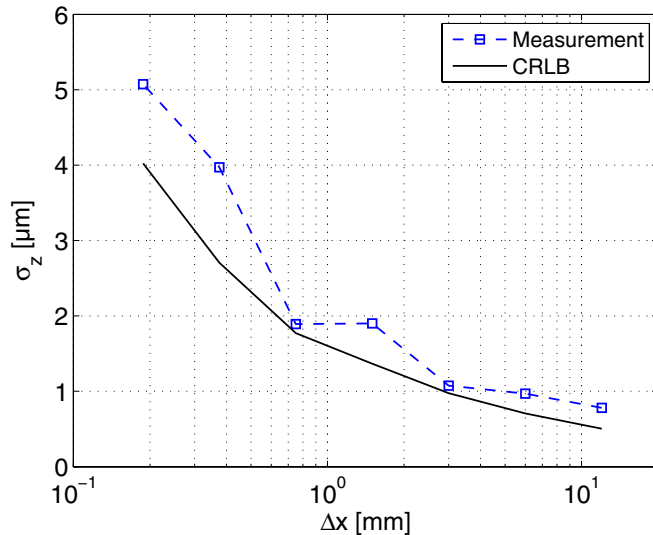


Figure 7. Experimentally obtained position standard uncertainty σ_z as a function of the lateral averaging length Δx on a moving rough test object surface (aluminum sheet) in comparison with the CRLB calculated via equation (30).

uncertainties revealing specific measuring features and the arising capabilities of the respective sensors. Moreover, it is a useful tool to judge and to compare the efficiency of different signal processing algorithms.

6. Conclusions

In this paper, a simple analytical expression has been derived for calculating the CRLB for the Doppler frequency estimation from scattered light signals of moving rough solid surfaces for the first time to the best of our knowledge. This is important for judging the potential of any specific laser Doppler sensor since the achievable measuring accuracy is fundamentally limited by the uncertainty of the Doppler frequency estimation in all laser Doppler techniques.

The CRLB represents the minimum achievable uncertainty of any unbiased estimator. The general approach for its derivation is well known. It requires an appropriate signal model that was deduced neglecting the effects of interference fringe spacing variations, object acceleration and the overlap between consecutive burst signals, which originate from dominant speckles passing through the interference fringe systems successively. In particular, the latter simplification is not entirely fulfilled in general, but it simplifies the calculations a lot since consecutive Doppler bursts can be treated independently accordingly. In future, it should be investigated if or how this simplification can be superseded. However, despite neglecting the overlap between consecutive Doppler bursts, the derived analytical CRLB formula agrees very well with experimental results, which confirms that this simplification is acceptable. In addition it was shown that the noise can be modeled collectively by a Gaussian distribution because of the large signal offset.

Using the general approach, first a generalized analytical expression for the CRLB for the Doppler frequency estimation

from a single burst signal was derived, which has been proven to be consistent and in accordance with previous works. From this result, the CRLB for the Doppler frequency estimation from scattered light signals of moving rough solid surfaces has been deduced making use of the additive nature of the Fisher information. The final result is a simple analytical expression, which shows directly the influences of certain system and signal parameters on the minimum attainable measurement uncertainty.

In order to demonstrate the validity of this analytical result, a comparison with experimental data measured on a moving piece of aluminum sheet was carried out, in which four different signal processing techniques have been used for Doppler frequency estimation. The obtained experimental results agree very well with the analytically derived CRLB. In particular, the outcomes of two of the signal processing techniques used exceed the calculated CRLB only by a factor of 1.3 on average indicating excellent efficiency of these techniques. On the other hand, this excellent agreement between experimental results and theory substantiates the validity and the correctness of the derived analytical CRLB formula. In addition, this experiment demonstrates that the CRLB is a valuable tool to evaluate the efficiency of signal processing techniques.

The main progress for science is that the derived CRLB formula allows an easy estimation of the minimum attainable measurement uncertainties of laser Doppler sensors on moving rough solid surfaces for the first time. In addition, it directly shows the influences of certain system and signal parameters on the measurement uncertainty. This has been discussed exemplarily for LDV velocity measurements and for position measurements with a special laser Doppler distance sensor. Consequently, the derived analytical CRLB enables us to reveal specific measuring features and arising capabilities of different laser Doppler sensors on rough moving surfaces.

Acknowledgments

The authors thank the Deutsche Forschungsgemeinschaft (DFG) for their financial support (project Cz 55/19-1).

Appendix A. CRLB for Doppler frequency estimation from a single burst signal

A.1. CRLB derivation

For deriving the CRLB, we start with the general signal model (see equation (4)) including the low-frequency part. Replacing A by \hat{A}/γ , it can be rewritten as

$$\tilde{m}_s[k] = \hat{A} e^{-\frac{2f_D^2(k/f_s - t_0)^2}{w^2}} [\alpha + \cos(2\pi f_D(k/f_s - t_0))],$$

$$k = 0, \dots, N_0 - 1, \quad (\text{A.1})$$

with $\alpha = 1/\gamma$. This signal model has to be inserted into the general approach described in subsection 3.1 together with the vector of unknown parameters $\vec{a}_s = (f_D, \hat{A}, w, t_0)^T$. Taking into account the joint probability density function given in

equation (12), the log-likelihood function results into

$$\ln p(\vec{x}, \vec{a}_s) = -\frac{1}{2\sigma_n^2} \sum_{k=0}^{N_0-1} (x[k] - \tilde{m}_s[k])^2 - \frac{N_0}{2} \ln(2\pi\sigma_n^2). \quad (\text{A.2})$$

Inserting this function into equation (14), the following relation is obtained for the elements of the Fisher information matrix [2, 17, 18]:

$$\mathbf{I}_{hj} = -E \left\{ \frac{\partial^2 \ln p(\vec{x}, \vec{a}_s)}{\partial a_h \partial a_j} \right\} = \frac{1}{\sigma_n^2} \sum_{k=0}^{N_0-1} \left(\frac{\partial \tilde{m}_s[k]}{\partial a_h} \frac{\partial \tilde{m}_s[k]}{\partial a_j} \right), \quad h, j \in \{1, 2, 3, 4\}. \quad (\text{A.3})$$

The partial derivatives of the signal model represented by equation (A.1) with respect to the unknown parameters contained in \vec{a}_s are

$$\frac{\partial \tilde{m}_s[k]}{\partial f_D} = -\hat{A} e^{-\frac{2f_D^2(k/f_s - t_0)^2}{w^2}} \left[\frac{4f_D(k/f_s - t_0)^2}{w^2} (\alpha + \cos \beta) + 2\pi(k/f_s - t_0) \sin \beta \right] \quad (\text{A.4})$$

$$\frac{\partial \tilde{m}_s[k]}{\partial \hat{A}} = e^{-\frac{2f_D^2(k/f_s - t_0)^2}{w^2}} [\alpha + \cos \beta] \quad (\text{A.5})$$

$$\frac{\partial \tilde{m}_s[k]}{\partial w} = \hat{A} e^{-\frac{2f_D^2(k/f_s - t_0)^2}{w^2}} [\alpha + \cos \beta] \frac{4f_D^2(k/f_s - t_0)^2}{w^3} \quad (\text{A.6})$$

$$\frac{\partial \tilde{m}_s[k]}{\partial t_0} = \hat{A} e^{-\frac{2f_D^2(k/f_s - t_0)^2}{w^2}} \left[\frac{4f_D^2(k/f_s - t_0)}{w^2} (\alpha + \cos \beta) + 2\pi f_D \sin \beta \right] \quad (\text{A.7})$$

using the abbreviation $\beta = 2\pi f_D(k/f_s - t_0)$. The next step is to insert these derivatives into equation (A.3) to calculate the elements of the Fisher information matrix. The arising sums can be transformed to integrals according to

$$\begin{aligned} \sum_{k=0}^{N_0-1} g(k/f_s - t_0) &= f_s \sum_{k=0}^{N_0-1} g(k/f_s - t_0) \frac{1}{f_s} \\ &\approx f_s \int_0^{T_b} g(t - t_0) dt \approx f_s \int_{-T_b/2}^{T_b/2} g(t) dt \end{aligned} \quad (\text{A.8})$$

assuming that the sampling rate f_s is large compared to the Doppler frequency f_D and that $t_0 \approx T_b/2$ with $T_b = N_0/f_s$ (cf section 2.2, in particular equation (8) and figure 3). Hence, integrals of the form

$$\int_{-T_b/2}^{T_b/2} e^{-\frac{4f_D^2 t^2}{w^2}} t^n [K + \cos(q2\pi f_D t)] dt \approx K \int_{-T_b/2}^{T_b/2} e^{-\frac{4f_D^2 t^2}{w^2}} t^n dt \quad \text{with } n \in \{0, 1, 2, 3, 4\}, \quad q \in \{1, 2\}, \quad K \geq 0.5 \quad (\text{A.9})$$

are obtained, in which the products of the harmonic function and the exponential function can be neglected since the harmonic function oscillates faster than the decay of the exponential function due to $w \gg 1$. Note that $2w = N_{\text{fringes}}$ denotes the number of interference fringes within the

measurement volume which is usually in the range of 10–50. Since $\eta = T_b/T_w$ (see below) does not approach zero in our case, also the integrals $\int_{-T_b/2}^{T_b/2} e^{-\frac{4f_D^2 t^2}{w^2}} t^n \sin(q2\pi f_D t) dt$, $n \in \{1, 3\}$ and $q \in \{1, 2\}$, can be neglected compared to the other terms in the residual expressions. The solutions of the remaining integrals can be found in common formularies. As a result, we obtain the following Fisher information matrix:

$$\mathbf{I} \approx \frac{\sqrt{\pi} f_s \kappa}{2\sigma_n^2} \begin{pmatrix} \frac{3\hat{A}^2 w}{8f_D^3} \left[c_3 + \frac{2\pi^2 w^2}{3\kappa} c_2 \right] & -\frac{\hat{A} w}{4f_D^2} c_2 \\ -\frac{\hat{A} w}{4f_D^2} c_2 & \frac{w}{2f_D} c_1 \\ -\frac{3\hat{A}^2}{8f_D^2} c_3 & \frac{\hat{A}}{4f_D} c_2 \\ 0 & 0 \\ -\frac{3\hat{A}^2}{8f_D^2} c_3 & 0 \\ \frac{\hat{A}}{4f_D} c_2 & 0 \\ \frac{3\hat{A}^2}{8w f_D} c_3 & 0 \\ 0 & \frac{\hat{A}^2 f_D}{w} \left[c_2 + \frac{2\pi^2 w^2}{\kappa} c_1 \right] \end{pmatrix} \quad (\text{A.10})$$

with

$$\kappa = \kappa(\alpha) = 2\alpha^2 + 1 \quad (\text{A.11})$$

$$c_1 = c_1(\eta) = \text{erf}(2\eta) \quad (\text{A.12})$$

$$c_2 = c_2(\eta) = \text{erf}(2\eta) - \frac{4\eta}{\sqrt{\pi}} e^{-4\eta^2} \quad (\text{A.13})$$

$$c_3 = c_3(\eta) = \text{erf}(2\eta) - e^{-4\eta^2} \left(\frac{4\eta}{\sqrt{\pi}} + \frac{32\eta^3}{3\sqrt{\pi}} \right) \quad (\text{A.14})$$

$$\eta = \frac{T_b}{T_w} = \frac{f_D T_b}{2w}. \quad (\text{A.15})$$

The parameter η defines the ratio between the signal duration T_b and the $1/e^2$ width of the Gaussian burst envelope $T_w = 2w_t = 2w/f_D$. If the signal duration is large compared to the burst width ($T_b \gg T_w$), η becomes $\gg 1$ resulting in $c_1 \approx c_2 \approx c_3 \approx 1$. Finally, the CRLB for the Doppler frequency estimation from a single burst signal is determined by calculating the first diagonal element of the inverse \mathbf{I}^{-1} of the Fisher information matrix (cf equation (15)) resulting in

$$\begin{aligned} \text{var}(\hat{f}_D) \geq \text{CRLB}_s(\hat{f}_D) &= [\mathbf{I}^{-1}]_{11} = \frac{8\sigma_n^2 f_D^3}{\sqrt{\pi} \pi^2 f_s \hat{A}^2 w^3 c_2(\eta)} \\ &= \frac{64\sigma_n^2}{\sqrt{\pi} \pi^2 f_s \hat{A}^2 T_w^3 c_2(\eta)} \end{aligned} \quad (\text{A.16})$$

taking into account the relation $T_w = \frac{2w}{f_D}$.

Up to now, we considered the general signal model including the low-frequency part according to equation (A.1).

Neglecting this low-frequency part means setting $\alpha = 0$. The only impact of this definition on the above equations is that $\kappa(\alpha = 0) = 1$. However, this does not change the result of equation (A.16) since the parameter κ is not contained in this equation but canceled out in the calculations before. Hence, the result of equation (A.16) is valid for the signal model from equation (5) too. Consequently, the low-frequency part of the burst signal does not influence the CRLB of the Doppler frequency estimation and can be neglected accordingly. Therefore, we can define $\alpha = 0$ in the following as well as for our considerations throughout this paper.

As a last step, equation (A.16) should be rewritten by means of the SNR, which is very convenient for comparisons with experimental results (cf section 4). The SNR is defined by

$$\text{SNR}_s = \frac{\overline{P_s}}{\sigma_n^2} \quad (\text{A.17})$$

as the ratio between the average signal power $\overline{P_s}$ and the noise power σ_n^2 . The average power of the Doppler burst signal $\overline{P_s}$ can be calculated using equation (5) (or equation (A.1) with $\alpha = 0$) as

$$\begin{aligned} \overline{P_s} &= \frac{1}{T_b} \int_{-T_b/2}^{T_b/2} m_s(t)^2 dt = \frac{\hat{A}^2}{T_b} \int_{-T_b/2}^{T_b/2} e^{-\frac{4f_D^2 t^2}{w^2}} \cos^2(2\pi f_D t) dt \\ &= \frac{\sqrt{\pi} \hat{A}^2 w}{4T_b f_D} \left\{ \text{erf}\left(\frac{T_b f_D}{w}\right) \right. \\ &\quad \left. + \frac{1}{2} e^{-\pi^2 w^2} \left[\text{erf}\left(\frac{T_b f_D}{w} + j\pi w\right) + \text{erf}\left(\frac{T_b f_D}{w} - j\pi w\right) \right] \right\} \\ &\ll \text{erf}(T_b f_D / w) \\ &\approx \frac{\sqrt{\pi} \hat{A}^2}{8\eta} \text{erf}(2\eta) \end{aligned} \quad (\text{A.18})$$

with $\frac{T_b f_D}{w} = 2\eta$. The last term can be neglected since usually $\eta > 0.1$ and $w \gg 1$. Inserting equations (A.18) and (A.17) into equation (A.16) and using the relation $\eta = \frac{T_b}{T_w} = \frac{N_0}{f_s T_w}$ with $T_b = \frac{N_0}{f_s}$, we obtain

$$\begin{aligned} \text{var}(\hat{f}_D) \geq \text{CRLB}_s(\hat{f}_D) &= \frac{8 \text{erf}(2\eta)}{\pi^2 f_s \eta T_w^3 \text{SNR}_s c_2(\eta)} \\ &= \frac{8 c(\eta)}{\pi^2 N_0 T_w^2 \text{SNR}_s} \end{aligned} \quad (\text{A.19})$$

with the parameter

$$c(\eta) = \frac{\text{erf}(2\eta)}{c_2(\eta)} = \frac{\text{erf}(2\eta)}{\text{erf}(2\eta) - \frac{4\eta}{\sqrt{\pi}} e^{-4\eta^2}}. \quad (\text{A.20})$$

A.2. Effect of reducing number of unknown parameters

Because of its importance, the influence of choosing the unknown parameters is briefly discussed in the following. In the previous subsection, all four unknown parameters $\vec{a}_s = (f_D, \hat{A}, w, t_0)^T$ were taken into account.

If we assume instead that e.g. the half-width w of the Gaussian signal envelope is known corresponding to $\vec{a}_s = (f_D, \hat{A}, t_0)^T$, the 3rd line and the 3rd row of the Fisher information matrix in equation (A.10) drop out. As a result, the first diagonal element of the inverse matrix becomes

$$\begin{aligned} [\mathbf{I}^{-1}]_{11} &= \frac{16\sigma_n^2 f_D^3 c_1}{\sqrt{\pi} f_s \hat{A}^2 w \kappa(\alpha) [3c_1 c_3 - c_2^2 + \frac{2\pi^2 w^2}{\kappa(\alpha)} c_1 c_2]} \\ &\approx \frac{16\sigma_n^2 f_D^3 c_1}{\sqrt{\pi} f_s \hat{A}^2 w \kappa(\alpha) [\frac{2\pi^2 w^2}{\kappa(\alpha)} c_1 c_2]} = \frac{8\sigma_n^2 f_D^3}{\sqrt{\pi} \pi^2 f_s \hat{A}^2 w^3 c_2}. \end{aligned} \quad (\text{A.21})$$

Despite that the final result equals equation (A.16), the approximation in the second line of equation (A.21) is only valid for $\gamma \gg 0$, i.e. $\gamma \gtrsim 0.5$, because only then is the expression $\frac{2\pi^2 w^2}{3\kappa(\alpha)} \gg 1$ due to $w \gg 1$ and, consequently, the first two summands in the square bracket expression in the denominator can be neglected because of $3c_1 c_3 - c_2^2 < 3c_1 c_2$ since $c_1 > c_2 > c_3$. Thus, only if the modulation depth γ of the burst signal is high enough, are both results equal and the knowledge of the Gaussian envelope width w does not influence the CRLB for the Doppler frequency estimation. Otherwise, the result would differ from equation (A.16) and, in particular, the low-frequency signal part could not be neglected for the CRLB calculation since $\kappa(\alpha)$ would not cancel out from equation (A.21). Similar behavior emerges if the burst amplitude \hat{A} is assumed to be a known parameter. However, since all four parameters $\vec{a}_s = (f_D, \hat{A}, w, t_0)^T$ are usually not known in practice, it is important to consider all of them as unknown in order to obtain correct and universally valid results.

A.3. Comparison of our results with previous work

In [18], the following CRLB for the velocity estimation from a single burst signal (particle number $N_p = 1$) has been analytically derived for the special case when the burst duration T_b is large compared to the Gaussian envelope temporal width T_w ($T_b \gg T_w$) (see [18], table D.6):

$$\text{var}(\hat{v}_x) \geq \text{CRLB}_{s, \text{Fischer}}(\hat{v}_x) = \frac{2d^2 v^2}{\pi^2 w_x^2 N_0 \text{SNR}_s}. \quad (\text{A.22})$$

Unlike the original formula in [18], the term $(2 + \gamma^2)/\gamma^2$ was set to 1 here since the SNR was defined in a different way in [18] including the low-frequency signal part. Taking into account $\text{var}(f_D) = \text{var}(v_x)/d^2$ and $\frac{v_x}{w_x} = \frac{f_D d}{w d} = \frac{f_D}{w} = \frac{2}{T_w}$, equation (A.22) turns into

$$\text{var}(\hat{f}_D) \geq \text{CRLB}_{s, \text{Fischer}}(\hat{f}_D) = \frac{8}{\pi^2 N_0 T_w^2 \text{SNR}_s}, \quad (\text{A.23})$$

which is in perfect agreement with the result from equation (A.19), because $c(\eta) = 1$ for $T_b \gg T_w$ or $\eta \gg 1$.

A further comparison will be drawn with the CRLB for the Doppler frequency estimation calculated by Besson *et al* [15], who neglected the low-frequency signal part from the beginning and who considered w to be a known parameter.

With $\tilde{f}_D = f_D/f_s$, the dimensionless formula (cf [15], equation (29))

$$\text{CRLB}_{s,\text{Besson}}(\hat{f}_D) \approx \frac{8\sigma_n^2 \tilde{f}_D^3 \alpha_B^3}{\sqrt{\pi} \hat{A}^2 (\alpha_B^2 + \pi^2)} \quad (\text{A.24})$$

is derived. Inserting $\alpha_B = 1/w$ into this equation and non-dimensionalizing it using $\tilde{f}_D = f_D/f_s$ and the relation $\text{CRLB}_{s,\text{Besson}}(\hat{f}_D) = \text{CRLB}_{s,\text{Besson}}(\hat{f}_D)/f_s^2$, we obtain

$$\begin{aligned} \text{CRLB}_{s,\text{Besson}}(\hat{f}_D) &\approx \frac{8\sigma_n^2 f_D^3}{\sqrt{\pi} \left(\frac{1}{w^2} + \pi^2\right) \hat{A}^2 f_s w^3} \\ &\approx \frac{8\sigma_n^2 f_D^3}{\sqrt{\pi} \pi^2 \hat{A}^2 f_s w^3}, \end{aligned} \quad (\text{A.25})$$

where the term $1/w^2$ can be neglected due to $w \gg 1$. This result is consistent with equation (A.16) because Besson *et al* assumed $T_b \rightarrow \infty$ and, in this case, $c_2 = 1$. However, in contrast to equation (A.16), the calculations of Besson *et al* are not universally valid, but they imply a high modulation depth of the burst signal (see the previous subsection) and $T_b \gg T_w$ additionally.

Finally, we compare our results with the calculations of Sobolev *et al* [17] since they took into account also a finite signal duration T_b , even if their signal model comprising two harmonic signals with $\pi/2$ phase shift and stochastically independent noises is questionable and not correct in general. They derived the following CRLB in terms of the angular Doppler frequency ω_D (cf [17], equations (31) and (32)):

$$\text{CRLB}_{s,\text{Sobolev}}(\hat{\omega}_D) = \frac{\sigma_n^2 f_s^2 \alpha_S}{\hat{A}^2 (N_0 - 1)^3} \approx \frac{\sigma_n^2 f_s^2 \alpha_S}{\hat{A}^2 N_0^3}, \quad (\text{A.26})$$

with

$$\begin{aligned} \alpha_S &= \frac{8\tilde{\eta}^3}{\frac{\sqrt{\pi}}{2} \text{erf}(\tilde{\eta})(1 + 3\xi^2) - \tilde{\eta} e^{-\tilde{\eta}^2} (1 + \xi^2 (3 + 2\tilde{\eta}^2))} \\ &= \frac{128\eta^3}{\sqrt{\pi} [\text{erf}(2\eta)(1 + 3\xi^2) - \frac{4\eta}{\sqrt{\pi}} e^{-4\eta^2} (1 + \xi^2 (3 + 8\eta^2))]} \\ &\approx \frac{128\eta^3}{\sqrt{\pi} [\text{erf}(2\eta) - \frac{4\eta}{\sqrt{\pi}} e^{-4\eta^2}]}, \end{aligned} \quad (\text{A.27})$$

with $\tilde{\eta} = 2\eta$. The approximation of equation (A.27) is permitted since $\xi^2 = \frac{1}{2\pi^2 w^2} \ll 1$ because of $w \gg 1$. With $\text{CRLB}_{s,\text{Sobolev}}(\hat{f}_D) = \text{CRLB}_{s,\text{Sobolev}}(\hat{\omega}_D)/(4\pi^2)$ and $\frac{f_s \eta}{N_0} = \frac{\eta}{T_b} = \frac{1}{T_w}$, the result of Sobolev *et al* can be transformed into

$$\text{CRLB}_{s,\text{Sobolev}}(\hat{f}_D) \approx \frac{32\sigma_n^2}{\sqrt{\pi} \pi^2 \hat{A}^2 f_s T_w^3 c_2(\eta)}, \quad (\text{A.28})$$

which equals the result from equation (A.16) except for a factor of 2. This is caused by the fact that Sobolev *et al* assumed two harmonic signals with stochastically independent noises which is not valid in general, e.g. for quadrature signals and noises due to photodetection that are not stochastically independent. By considering only one signal instead as done for deriving equation (A.16), the Fisher information halves and, thus, the corresponding CRLB doubles.

In conclusion, our results are consistent with the results of previous works. However, the derivation described in

appendix A.1 provides a more general and universally valid way of calculating the CRLB of the Doppler frequency estimation from a single burst signal.

References

- [1] Yeh Y and Cummins H Z 1964 Localized fluid flow measurements with an He-Ne laser spectrometer *Appl. Phys. Lett.* **4** 176–8
- [2] Albrecht H-E, Borys M, Damaschke N and Tropea C 2003 *Laser Doppler and Phase Doppler Measurement Techniques* (Berlin: Springer)
- [3] Czarske J W 2006 Laser Doppler velocimetry using powerful solid-state light sources *Meas. Sci. Technol.* **17** R71–91
- [4] Truax B E, Demarest F C and Sommargren G E 1984 Laser Doppler velocimeter for velocity and length measurements of moving surfaces *Appl. Opt.* **23** 67–73
- [5] Stork W, Wagner A and Kunze C 2001 Laser-Doppler sensor system for speed and length measurements at moving surfaces *Proc. SPIE* **4398** 106–15
- [6] Czarske J, Büttner L, Razik T and Müller H 2002 Boundary layer velocity measurements by a laser Doppler profile sensor with micrometre spatial resolution *Meas. Sci. Technol.* **13** 1979–89
- [7] Pfister T, Büttner L and Czarske J 2005 Laser Doppler profile sensor with sub-micrometre position resolution for velocity and absolute radius measurements of rotating objects *Meas. Sci. Technol.* **16** 627–41
- [8] Pfister T, Büttner L and Czarske J 2005 In-process shape and roundness measurements at turning machines using a novel laser Doppler profile sensor *Proc. SPIE* **5776** 44–55
- [9] Pfister T, Büttner L, Czarske J, Krain H and Schodl R 2006 Turbo machine tip clearance and vibration measurements using a fibre optic laser Doppler position sensor *Meas. Sci. Technol.* **17** 1693–705
- [10] Pfister T, Günther P, Nöthen M and Czarske J 2010 Heterodyne laser Doppler distance sensor with phase coding measuring stationary as well as laterally and axially moving objects *Meas. Sci. Technol.* **21** 025302
- [11] Shirai K, Pfister T, Büttner L, Czarske J, Müller H, Becker S, Lienhart H and Durst F 2006 Highly spatially resolved velocity measurements of a turbulent channel flow by a fiber-optic heterodyne laser-Doppler velocity-profile sensor *Exp. Fluids* **40** 473–81
- [12] Bayer C, Shirai K, Büttner L and Czarske J 2008 Measurement of acceleration and multiple velocity components using a laser Doppler velocity profile sensor *Meas. Sci. Technol.* **19** 055401
- [13] König J, Voigt A, Büttner L and Czarske J 2010 Precise micro flow rate measurements by a laser Doppler velocity profile sensor with time division multiplexing *Meas. Sci. Technol.* **21** 074005
- [14] Rife D and Boorstyn R 1974 Single tone parameter estimation from discrete-time observations *IEEE Trans. Inf. Theory* **20** 591–8
- [15] Besson O and Galtier F 1996 Estimating particles velocity from laser measurements: maximum likelihood and Cramer–Rao bounds *IEEE Trans. Signal Process.* **44** 3056–68
- [16] Shu W Q 2001 Cramer–Rao bound of laser Doppler anemometer *IEEE Trans. Instrum. Meas.* **50** 1770–2
- [17] Sobolev V S and Feshenko A A 2006 Accurate Cramer–Rao bounds for a laser Doppler anemometer *IEEE Trans. Instrum. Meas.* **55** 659–65
- [18] Fischer A, Pfister T and Czarske J 2010 Derivation and comparison of fundamental uncertainty limits for

- laser-two-focus velocimetry, laser Doppler anemometry and Doppler global velocimetry *Measurement* **43** 1556–74
- [19] Drain L E 1980 *The Laser Doppler Technique* (Chichester: Wiley)
- [20] Agrawal G P 1997 *Fiber-Optic Communication Systems* 2nd edn (New York: Wiley)
- [21] Kay S M 1993 *Fundamentals of Statistical Signal Processing, Volume I: Estimation Theory* (Englewood Cliffs, NJ: Prentice-Hall)
- [22] Czarske J W 2001 Statistical frequency measuring error of the quadrature demodulation technique for noisy single-tone pulse signals *Meas. Sci. Technol.* **12** 597–614